Solar Phys (2014) 289:3773–3797
DOI 10.1007/s11207-014-0552-4

Solar Sources of Interplanetary Coronal Mass Ejections During the Solar Cycle 23/24 Minimum

E.K.J. Kilpua · M. Mierla · A.N. Zhukov · L. Rodriguez · A. Vourlidas · B. Wood

Received: 17 December 2013 / Accepted: 9 May 2014 / Published online: 10 June 2014

Abstract We examine solar sources for 20 interplanetary coronal mass ejections (ICMEs) observed in 2009 in the near-Earth solar wind. We performed a detailed analysis of coronagraph and extreme ultraviolet (EUV) observations from the *Solar Terrestrial Relations Observatory* (STEREO) and *Solar and Heliospheric Observatory* (SOHO). Our study shows that the coronagraph observations from viewpoints away from the Sun–Earth line are paramount to locate the solar sources of Earth-bound ICMEs during solar minimum. SOHO/LASCO detected only six CMEs in our sample, and only one of these CMEs was wider than 120°. This demonstrates that observing a full or partial halo CME is not necessary to observe the ICME arrival. Although the two STEREO spacecraft had the best possible configuration for observing Earth-bound CMEs in 2009, we failed to find the associated CME for four ICMEs, and identifying the correct CME was not straightforward even for some clear ICMEs. Ten out of 16 (63 %) of the associated CMEs in our study were "stealth" CMEs, *i.e.* no obvious EUV on-disk activity was associated with them. Most of our stealth CMEs also lacked on-limb EUV signatures. We found that stealth CMEs generally lack the leading bright front in coronagraph images. This is in accordance with previous studies that

E.K.J. Kilpua (✉)
Department of Physics, Division of Geophysics and Astronomy, University of Helsinki, Helsinki, Finland
e-mail: Emilia.Kilpua@helsinki.fi

M. Mierla · A.N. Zhukov · L. Rodriguez
Solar-Terrestrial Center of Excellence – SIDC, Royal Observatory of Belgium, Av. Circulaire 3, 1180 Brussels, Belgium

M. Mierla
Institute of Geodynamics of the Romanian Academy, Jean-Louis Calderon 19-21, 020032 Bucharest-37, Romania

A.N. Zhukov
Skobeltsyn Institute of Nuclear Physics, Moscow State University, 119992 Moscow, Russia

A. Vourlidas · B. Wood
Space Science Division, Naval Research Laboratory, Washington, DC 20375, USA

argued that stealth CMEs form more slowly and at higher coronal altitudes than non-stealth CMEs. We suggest that at solar minimum the slow-rising CMEs do not draw enough coronal plasma around them. These CMEs are hence difficult to discern in the coronagraphic data, even when viewed close to the plane of the sky. The weak ICMEs in our study were related to both intrinsically narrow CMEs and the non-central encounters of larger CMEs. We also demonstrate that narrow CMEs (angular widths $\leq 20^{\circ}$) can arrive at Earth and that an unstructured CME may result in a flux rope-type ICME.

Keywords Coronal mass ejections · Solar wind · Corona · Interplanetary coronal mass ejection

1. Introduction

Coronal mass ejections (CMEs) are huge eruptions from the Sun that are of paramount importance for heliospheric and solar-terrestrial physics. CMEs drive practically all intense magnetospheric storms (*e.g.* Gosling *et al.*, 1991; Huttunen, Koskinen, and Schwenn, 2002; Zhang *et al.*, 2005); they remove closed magnetic flux and helicity from the Sun, as reported by Owens *et al.* (2007), modulate cosmic-ray intensity, as described by Cane (2000), accelerate solar energetic particles (*e.g.* Reames, 1999), and affect the structure of slow–fast stream interaction regions (SIRs) and consequently the SIR-associated solar energetic particle events, as described by Gomez-Herrero *et al.* (2011). Therefore, understanding the CME properties and evolution in the heliosphere is a key research area.

Most of our remote knowledge on CMEs comes from coronagraph observations (*e.g.* Hundhausen *et al.*, 1984; St. Cyr *et al.*, 2000; Yashiro *et al.*, 2004), which are limited to within a few tens of solar radii [$R_{\odot}$] from the Sun. CMEs can be followed with heliospheric imagers (*e.g.* Eyles *et al.*, 2003; Harrison, Davis, and Eyles, 2005; Harrison *et al.*, 2009) to the orbit of Earth and beyond, but these observations are often difficult to interpret because of projection effects and the weakening of the CME signal as it travels away from the Sun (*e.g.* Lugaz, Manchester, and Gombosi, 2005). Connecting remote and interplanetary CME (ICME) observations is often ambiguous (*e.g.* Schwenn *et al.*, 2005; Möstl *et al.*, 2010): at solar maximum, several strong CMEs may be launched per day, which complicates the selection of unique CME–ICME pairs, while near solar minimum CMEs are more difficult to detect since they tend to be weaker than during the years of high solar activity, as reported by Vourlidas *et al.* (2011). Some CMEs may also erupt without leaving obvious signatures on the solar disk, as described by Robbrecht, Patsourakos, and Vourlidas (2009), Ma *et al.* (2010). These CMEs were called "stealth CMEs" by Robbrecht, Patsourakos, and Vourlidas (2009), who suggested that they start slowly and form higher up in the corona than CMEs whose source regions at the Sun are revealed by signatures such as EUV dimming, post-eruption arcades, erupting filaments, or EIT waves (*e.g.* Hudson and Cliver, 2001; Zhukov, 2007).

The solar minimum between Solar Cycles 23 and 24 was unusually extended and deep. In 2009 the monthly sunspot number was below five from January to November, but the ICME rate had increased significantly from its lowest values in 2007 – 2008; combining the near-Earth ICME observations from three catalogs [the *Wind* magnetic-cloud list (lepmfi.gsfc.nasa.gov/mfi/mag_cloud_S1.html; Lepping and Wu, 2010), the Richardson and Cane (R&C) ICME list (http://www.srl.caltech.edu/ACE/ASC/DATA/level3/icmetable2.htm; Richardson and Cane, 2010), and the UCLA ICME list (maintained at the ACE Science Center: http://www.srl.caltech.edu/ACE/ASC/; Jian *et al.*, 2006)] a total of five ICMEs

were reported in 2007, four in 2008, and 19 in 2009 (see also the discussion by Kilpua *et al.*, 2011a). However, only a few wide CMEs were identified by the *Large Angle Spectroscopic COronagraph* (LASCO: Brueckner *et al.*, 1995) onboard the *SOlar and Heliospheric Observatory* (SOHO) in 2009: one full halo (Howard *et al.*, 1982) and two partial-halo (angular width $>120°$) CMEs were reported in the LASCO catalog (cdaw.gsfc.nasa.gov/CME_list/; Yashiro *et al.*, 2004) and three partial halos in the automated SEEDs catalog (spaceweather.gmu.edu/seeds/; Olmedo *et al.*, 2008), while no wider CMEs were included in the automated CACTus catalog (sidc.oma.be/cactus/; Robbrecht and Berghmans, 2004). Note that neither the manual nor the automated method is perfect in its capability to identify CMEs, and therefore the CMEs included in different CME catalogs may differ significantly, in particular in the case of narrow and faint CMEs (*e.g.* Yashiro, Michalek, and Gopalswamy, 2008). Since halo and partial halo CMEs in LASCO images are considered as potential candidates for Earth-impacting CMEs, the lack of wide CMEs in 2009 raises the question of the origin of ICMEs in 2009.

It is well-known that CMEs are difficult to detect from the spacecraft towards which they are heading, because the Thomson-scattering emission is weaker for CME propagating away from the sky plane of the observer, as reported by Vourlidas and Howard (2006). In 2009 the *Solar Terrestrial Relations Observatory* (STEREO: Kaiser *et al.*, 2007) spacecraft had a suitable configuration to view Earth-directed CMEs. STEREO consists of two functionally identical spacecraft, with one of them (STEREO-A) leading the Earth and the other (STEREO-B) lagging the Earth in its orbit, with increasing angular separation ($45° \text{ year}^{-1}$). In 2009 the separation angle of STEREO-A with Earth varied from 43° to 68°, for STEREO-B this was from 46° to 64°. As a consequence, the STEREO spacecraft were able to observe Earth-directed CMEs as "limb" CMEs, and therefore it was expected that they would be able to capture the faint and narrow Earth-bound CMEs that might be missed by LASCO.

In this article we perform a systematic survey of CME sources for ICMEs observed in 2009, taking advantage of STEREO observations. We seek answers to the following questions: i) Can we find solar-disk and white-light counterparts for solar-minimum ICMEs when a wide-angle view-point from STEREO is available? ii) Are interplanetary counterparts of stealth CMEs different from those associated with non-stealth CMEs? And finally, iii) what do white-light and *in-situ* morphologies of CMEs have in common? In addition, one of the interesting questions that we address is whether solar sources for weak ICMEs as described by Feng *et al.* (2008) and Kilpua *et al.* (2009) are similar to those for larger ICMEs. That is to say, do they arise from similar initial coronal configurations, and do they have similar initiation mechanisms?

2. Data and Approach

The ICMEs analyzed in this article are listed in Table 1. They are gathered from the three online catalogs given in Section 1, and we added an ICME observed on 30 August 2009, discussed in detail by Nieves-Chinchilla *et al.* (2013). The *Wind* list contains only magnetic clouds, *i.e.* events that show a smoothly rotating magnetic field direction, which therefore are interpreted to contain magnetic-flux ropes. The UCLA and R&C lists also contain ICMEs that do not show coherent magnetic field rotation. The columns of Table 1 indicate the event number, shock/wave time (if observed), ICME leading edge time, the ICME list(s) where the ICME was included, ICME duration [ΔT], maximum magnetic field [$B_{\max}$], and maximum speed [[$V_{\max}$]]. The panel "P_t Group" gives the estimate for the spacecraft crossing distance from the ICME center (impact parameter) based on the temporal variations of the

Table 1 ICMEs and selected parameters. The last two columns only give the Kp maximum when Kp reached at least 4– and the Dst minimum only when Dst decreased to below −30 nT as a response to the ICME.

N	Shock/wave [UT]	ICME start [UT]	List[1]	ΔT[2] [hours]	B_{max}[3] [nT]	V_{max}[4] [km s^{-1}]	P_t group[5]	FR[6]	Kp max	Dst min [nT]
1	–	2 Jan, 6	W	9	7.0	400	2	FR	4–	–
2	18 Jan 22:05	19 Jan, 2	R	4	12.9	433	2	–	4	–
3	25 Jan 22:25	25 Jan, 22	A, R	10	11.1	333	nc	–	–	–
4	03 Feb 20:16	4 Feb, 1	A, R, W	17	11.3	385	2	FR	4–	–
5	11 Mar 23:25	12 Mar, 2	A, W	26	18.6	355	1	FR	5–	–32
6	–	3 Jun, 21	R	41	7.0	311	3	–	–	–
7	27 Jun, 12:15	27 Jun, 17	A, R, W	29	12.2	420	nc	FR	4	–
8	–	21 Jul, 4	A, R, W	25	8.0	335	nc	FR	6–	–83
9	–	5 Aug, 3	A	26	14.6	360	1	–	4	–
10	30 Aug, 01:40	30 Aug, 9	–	6	12.9	423	nc	–	6–	–
11	–	10 Sep, 10	W	30	6.3	306	2	FR	–	–
12	30 Sep, 02:10	30 Sep, 8	A, R, W	13	9.5	350	1	FR	–	–
13	–	12 Oct, 13	W	9	6.8	351	1	FR	–	–
14	–	16 Oct, 22	A	12	3.6	355	1	–	–	–
15	–	17 Oct, 21	A, W	18	3.7	323	1	FR	–	–
16	–	29 Oct, 3	A, R, W	32	11.4	357	1	FR	–	–34
17	31 Oct, 21:22	1 Nov, 11	W	22	8.5	334	2	FR	–	–
18	–	14 Nov, 11	A, R	26	8.2	328	2	–	–	–
19	12 Dec, 06:05	12 Dec, 21	A, R, W	25	8.2	287	1	FR	–	–
20	–	19 Dec, 13	R	28	5.2	439	3	–	–	–

[1]The online catalog where the ICME is included (A = UCLA ACE list, R = Richardson and Cane list, W = *Wind* magnetic-cloud list; see Section 2 for more details).

[2]ICME duration.

[3]Maximum magnetic field within the ICME.

[4]Maximum speed within the ICME.

[5]Estimate of the impact parameter based on the perpendicular-pressure profile (1 = central encounter, 2 = encounter from the intermediate distance, and 3 = edge encounter, nc = not clear, see Section 2 for details).

[6]"FR" indicates whether the ICME showed smooth magnetic field rotation.

total pressure (sum of the magnetic pressure and plasma thermal pressure) perpendicular to the magnetic field, as reported by Jian *et al.* (2006): in Group 1 the P_t profile has a central maximum (centrally crossed ICME), in Group 2 it has a plateau-like profile (crossing from intermediate distance from the center), and in Group 3 a gradual decrease after a sharp increase is observed (edge encounter). Panel FR indicates whether the ICME had a flux rope structure.

Table 1 shows that five ICMEs were included in all lists considered: six in two of them, and eight events were included only in one catalog. Previous studies (*e.g.* Richardson and Cane, 2010) have already revealed large discrepancies between ICME catalogs, as well as discrepancies during the years of high solar activity when ICMEs tend to be stronger and have larger widths than near solar minimum. We note that the identification of ICMEs is always subject to some level of ambiguity because there is no signature that is present in all ICMEs, and various signatures do not always occur simultaneously (*e.g.* Gosling, 1997; Zurbuchen and Richardson, 2006). In addition, different ICME lists emphasize different solar wind signatures. For example, the UCLA list uses temperature as one of their main identification criteria, the *Wind* list relies primarily on magnetic field signatures, and the R&C list emphasizes the variations of P_t. We have examined data of the solar wind magnetic field, the plasma, and suprathermal and composition data during the ICME intervals listed in the catalogs and confirm that they indeed represent ICME signatures in our judgement. For example, the first ICME in our data set, observed on 2 January 2009, is relatively weak and is only included in the *Wind* list. However, a careful inspection of solar wind measurements reveals a clear rotation of the magnetic field direction for about nine hours (but it is difficult to detect because the magnetic field magnitude is about at the same level as that of the surroundings) and a low proton temperature.

For each event we estimated the time when the corresponding CME left the Sun by assuming that it propagates into the heliosphere with the speed of the ICME leading edge. This approach is justified from the results by Kilpua *et al.* (2012), who showed that the ICME leading edge speed provides a relatively good estimate of the Sun-to-Earth travel time for slow CMEs during the recent solar minimum. We searched for CMEs within a three-day window around the estimated CME time; the main focus was on STEREO observations. The STEREO spacecraft carry two coronagraphs, which are part of the *Sun Earth Connection Coronal and Heliospheric Investigation* (SECCHI) instrument package as described by Howard *et al.* (2008b). The field of view of the inner coronagraph COR1 extends from 1.5 to 4 $R_\odot$, and the outer coronagraph COR2 has a field of view between 2.5 and 15 $R_\odot$. We also searched for the corresponding CMEs from LASCO movies. The LASCO coronagraphs in operation at the time of this study were C2 and C3, whose fields of view extend from 2.2 to 6 $R_\odot$, and from 3.7 to 32 $R_\odot$. We examined both normal and running-difference movies to extract the faint CMEs. Since all CMEs and ICMEs included in this work were relatively slow, we favored CMEs that were detected around the estimated time or earlier than CMEs detected after the estimated time. It does not seem plausible that an initially slow CME would have accelerated significantly after leaving the COR2 field of view and then decelerated before arriving at Earth. Instead, solar-minimum CMEs tend to start slowly, which can considerably increase their expected Sun-to-Earth travel times (see also the discussion below). Our first selection criterion was that the CMEs had to leave from the "correct" limb in STEREO-A and STEREO-B. At the time studied, STEREO-A should have seen Earth-directed CMEs on the east limb (position angles around 90°) and STEREO-B on the west limb (position angles around 270°).

We divided CMEs into flux rope CMEs (FR-CMEs) and unstructured "flow-like CMEs" based on their appearance in white-light coronagraph images. flux rope signatures in coronagraphic data are discussed extensively in Vourlidas *et al.* (2013). The classical three-part

CME described by Illing and Hundhausen (1985) consists of a bright front and a dark cavity with an embedded core. As discussed by Vourlidas *et al.* (2013), the cavity corresponds to the flux rope, which means that in most cases indirect proxies are needed to identify it. The authors argued that the bright front is the result of coronal pileup at the boundary of the erupting flux rope and can therefore be considered to signal the flux rope morphology, even when the cavity and the core are not observed. The other flux rope signatures discussed by Vourlidas *et al.* (2013) are concave upward "horns" outlining the bottom part of the flux rope.

For FR-CMEs we performed a multispacecraft forward-modeling (FM) analysis as described by Thernisien, Howard, and Vourlidas (2006) and Thernisien, Vourlidas, and Howard (2009). This technique is based on fitting a graduated cylindrical shell (GCS) flux rope model (Chen *et al.*, 1997; Thernisien, Howard, and Vourlidas, 2006) to white-light coronagraph images. The GCS model consists of a tubular section that forms the main body of the flux rope that is attached to two cones that correspond to the legs of the CME. The parameters of this geometrical model (angular width, height, location on the solar disk, *etc.*) are changed until the model visually best adjusts the observed CME. The FM fitting allowed us to estimate the CME direction of propagation in longitude and latitude, the cross-sectional area of the CME legs, the tilt angle around the axis of symmetry, and the half-angle between the legs. From these parameters, we were able to estimate whether the CME would intercept Earth (see Rodriguez *et al.*, 2011). For flow-like CMEs we estimated the propagation direction using geometrical triangulation, following Inhester (2006). The selected CME associations and their key information are given in Table 2, the reconstruction results are given in Table 3.

Finally, we used the *Heliospheric Imager* (HI) included in the STEREO/SECCHI package, as described by Howard *et al.* (2008b). The HI-1 view angle ranges from 4° to 24° elongation from Sun center; the HI-2 elongation ranges from 18° to 88°. The HI-2 fronts associated with the ICMEs were tracked backwards to HI-1 and were subsequently associated with the CMEs seen in COR2 (*e.g.* Wood and Howard, 2009; Wood, Howard, and Socker, 2010). The CMEs that were bright enough to be tracked with HI are indicated in the last column of Table 3.

For each CME we defined the plane-of-sky angular width (AW) and speed from COR2 measurements. As discussed in Section 1, in 2009 STEREO was expected to detect Earth-bound CMEs almost as limb CMEs, therefore speeds and AWs derived from STEREO images contribute relatively little to the projection effects (*e.g.* Hundhausen, 1993; Howard, Nandy, and Koepke, 2008a). The AW given in Table 2 is the mean AWs from two STEREO spacecraft. If either of the STEREO spacecraft detected a partial halo (AW $> 120°$), we used the AW measured from the other spacecraft. The speed given in Table 2 is that of the STEREO spacecraft that observed the higher speed. This is because projected speeds tend to be lower than the actual speeds (*e.g.* Howard, Nandy, and Koepke, 2008a).

We also performed a detailed survey of EUV disk activity using observations from the *EUV Imaging Telescope* (EIT: Delaboudinière *et al.*, 1995) and *Extreme UltraViolet Imager* (EUVI: Wülser *et al.*, 2004) instruments onboard SOHO and STEREO, respectively. Both EIT and EUVI monitor the Sun in four bandpasses centered on 171, 195, 284, and 304 Å. We searched for typical CME on-disk related signatures such as coronal dimming, EIT waves, prominence/filament eruptions, and post-eruption arcades (Hudson and Cliver, 2001; Zhukov, 2007).

We identified the times of the CMEs first appearance in each coronagraph field of view (COR2 or COR1) and selected the spacecraft (STEREO-A or -B) that first detected the CME. An earlier detection of a CME by, *e.g.*, STEREO-A than by STEREO-B indicates

Table 2 CME/EUV associations. The estimated solar time is based on the ICME leading edge speed (see Section 2). The observed CME time is the time when the CME first appeared in the COR2 field of view. The angular width (AW) of a CME is the mean value from the two STEREO spacecraft. When only one spacecraft was used, the spacecraft is indicated in parenthesis. CME speed is determined from STEREO/COR2 data and we have selected the higher speed (the spacecraft indicated in parenthesis: A = STEREO-A, B = STEREO-B).

N	CME time estimated [UT]	CME time observed [UT]	CME speed [km s^{-1}]	AW STEREO [°][1]	AW LASCO [°][2]	White-light type[3]	EUV activity[4]	EUV coordinates
1	28 Dec 22	28 Dec 5	430 (B)	26	–	flow	stealth	–
2	15 Jan 2	14 Jan 3	470 (A)	75 (A)	104	FR (F)	dimming, EP, PEA	N55E30
3	21 Jan 11	21 Jan 17	390 (B)	60 (B)	73	FR (F)	PEA-like brightening	–
4	30 Jan 7	30 Jan 8	300 (A)	53	–	FR	stealth	
5	7 Mar 4	none	–	–	–	–	–	–
6	29 May 12	none	–	–	–	–	no activity	–
7	23 Jun 9	23 Jun 7	220 (B)	50 (B)	39	FR (F)	dimming, EP	S20E22
8	15 Jul 22	15 Jul 15	220 (A)	28	–	flow	stealth	–
9	31 Jul 8	31 Jul 5	300 (A)	53	–	FR (F)	stealth	–
10	26 Aug 8	25 Aug 10	300 (A)	45	67	FR	stealth	–
11	4 Sep 18	3 Sep 8	280 (A)	–	48	FR	stealth	–
12	25 Sep 8	25 Sep 16	330 (A)	13	–	flow	stealth	–
13	7 Oct 20	none	–		–	–	no activity	–
14	11 Oct 20	none	–		–	–	no activity	–
15	12 Oct 1	12 Oct 7	NA	15 (A)	–	flow	dimming, EP, PEA, wave	N20W10
16	24 Oct 15	23 Oct 16	data gap	50 (A)	57	FR	stealth	–
17	27 Oct 6	27 Oct 17	400 (A)	20	–	FR	stealth	–
18	9 Nov 5	9 Nov 17	280 (A)	35	–	FR (F)	dimming, EP, PEA	N55W04
19	6 Dec 18	6 Dec 14	190 (B)	33	–	FR	stealth	–
20	Dec 15 14	16 Dec 2	520 (A)	55	360	FR (F)	dimming, PEA, wave	N33W10

[1] Angular width of the CME determined from STEREO/COR2 data.

[2] Angular width of the CME determined from LASCO (if visible).

[3] White-light morphology of the CME (FR = flux rope; "F" in parenthesis indicates that a bright front was observed).

[4] EUV activity related to the CME eruption. EP = eruptive prominence, PEA = post eruptive arcade, and "stealth" means that no obvious activity was related to a CME.

Table 3 Results of the 3D reconstruction analysis (see Section 2). Events marked with "*" are flow-like CMEs (see Table 2) for which we have used triangulation to determine the propagation direction. The flux rope CME reconstruction results are based on the forward modeling (FM). In the two last columns "NA" indicates that the white-light feature was too faint for FM/HI analysis.

N	Time[1] [UT]	Long[2] [°]	Lat[3] [°]	Tilt [°]	Ratio	α[4] [°]	Hit[5]	HI[6]
	2008							
1	28 Dec 10:08*	8	11	–	–	–	NA	NA
	2009							
2	14 Jan 13:07	–29	1	−11	0.27	27	B, E	B, E
3	22 Jan 02:37	19	−4	−3	0.34	25	A, E	A, E
4	30 Jan 17:07*	3	−2	–	–	–	NA	–
5	–	–	–	–	–	–	–	–
6	–	–	–	–	–	–	–	–
7	23 Jun 09:37	19	–10	–30	0.18	15	E	E
8	16 Jul 01:08*	–2	4	–	–	–	NA	E
9	31 Jul 10:37	8	14	2	0.23	21	E	NA
10	25 Aug[7]							
11	4 Sep 05:24	–7	5	3		–	NA	NA
12	25 Sep 20:24	8	2	–	–	–	–	E
13	–	–	–	–	–	–	–	–
14	–	–	–	–	–	–	–	–
15	12 Oct 11:24	12	2	–	–	–	NA	NA
16	Data gap	–	–	–	–	–	–	–
17	27 Oct 23:24	6	3	–10	0.12	13	E	E
18	9 Nov 23:24	2	5	6	0.18	9	E	E
19	6 Dec 21:39	–8	–6	–29	0.18	10	E	E
20	15 Dec 08:54	–16	13	8	0.27	22	E	E

[1]Time when forward modeling or triangulation was performed.

[2]Longitude of the CME progagation direction.

[3]Latitude of the CME propagation direction.

[4]CME half-width.

[5]The spacecraft that the CME encountered according to forward modeling (A = STEREO-A, B = STEREO-B, E = Earth).

[6]The spacecraft that the CME encountered according to STEREO/*Heliospheric Imager* analysis.

[7]See Nieves-Chincilla *et al.* 2013.

that the CME source region is situated closer to the limb as seen from STEREO-A. This gives a rough idea about the heliographic longitude of the source region. After that we inspected the EUVI data in the 195 Å and 304 Å passbands up to ten hours before the CME first appearance in the COR2 or COR1 (when visible) field of view. The lower edge of the COR2 field of view is situated around 2.5 solar radii, which means that a CME would need to propagate at an unrealistically low speed (around 30 km s^{-1}) for its start to lie outside the ten-hour window. We searched for EUV activity (the CME signatures mentioned above) in this time window using plain, running-difference, and base-difference EUVI images. The

procedure was repeated for the second STEREO spacecraft. In many cases, the same source region was identified in the data taken by the two spacecraft.

We carefully avoided misidentification of CME signatures in the low corona. Since the early days of the SOHO mission it has been known that small-scale activity is omnipresent in the EUV quiet Sun (*e.g.* Gurman *et al.*, 1998), with small-scale weak brightenings and dimmings occurring all the time. Innes *et al.* (2009) reported a rate of about 1400 eruptions per day on supergranulational scales. Because there are significantly fewer CMEs (fewer than ten per day in 2009) than there are small-scale phenomena, this small-scale activity is not a reliable indicator of the CME source region in the low corona. In many cases we relied on the detection of one of the CME signatures mentioned above: EUV dimmings (typically with the size of an active region or larger), erupting prominences/filaments (with the material clearly moving out of the field of view), post-eruption arcades, and ejection-like limb signatures (*e.g.* loop opening without a noticeable dimming). These large-scale signatures are well-known manifestations of the CME eruption process (*e.g.* Hudson and Cliver, 2001; Zhukov, 2007), but they lack one-to-one association with CMEs (*e.g.* Nitta *et al.*, 2014). A CME may be associated with only some of these signatures, but none of them is absolutely required. However, if any of these CME signatures is observed, then there generally should be a CME eruption detectable by a coronagraph from a favorable perspective (close to the limb). In other words, these CME signatures represent sufficient but not necessary conditions for a CME occurrence. Other EUV phenomena that may be CME-associated either can be reduced to one of the above-mentioned signatures (*e.g.* sigmoid-to-arcade restructuring always exhibits a post-eruption arcade), or they are not sufficiently conclusive CME signatures. For example, flares, which are often seen in association with CMEs, are not sufficiently conclusive CME signatures because there are many flares without an associated CME.

If no on-disk EUV signature was observed in the low corona by EUVI and EIT, we classified the CME as a stealth CME. However, some EUV signatures of stealth CMEs can be observed in the low corona above the limb. These are typically limb dimmings or ejection-like limb signatures such as loop opening. Visibility of CME signatures above the limb in the absence of on-disk signatures indicates that in these cases the CME develops so slowly that it is very difficult to see its trace on the solar disk in EUV. CME signatures could be better seen in EUV against a simpler background above the limb, but the solar disk in EUV passbands is too complex and too dynamic for the same motion of structures to be visible on it. The results of the detailed analysis of stealth CMEs in COR1 and EUV observations are gathered in Table 4 (see more detailed explanation in Section 4.3).

3. Example Events

In this section we describe two example events. The first example shows an ICME for which the correct CME association was easily made with the confirmation from the FM analysis. The second event illustrates a clear ICME for which finding the correct white-light association was complicated.

3.1. Example 1: 27 October – 2 November 2009

Figure 1 shows the five-minute-averaged near-Earth heliospheric data base (OMNI) measurements for Event 17. The ICME interval is bounded by a pair of solid lines and it extended from 1 November 11 UT to 2 November 10 UT. The dashed line marks a leading

Table 4 Stealth CMEs and their low-corona signatures. The table indicates the times when the CME was first detected in the STEREO/COR2 and COR1 fields of view and in EUVI on limb. The times are approximate because the events were slow and faint or occurred close in time to previous flows. For the events marked with an asterisk in columns 7 or 8, erupting signatures were found in EUVI images, but the position of this tentative source region did not correspond to the CME appearance in the coronagraph field of view.

N	Date	COR2-A time [UT]	COR2-B time [UT]	COR1-A time [UT]	COR1-B time [UT]	EUVI-A signatures	EUVI-B[1] signatures
1	28 Dec 2008	05:00	04:30	04:05	not clearly visible	nothing	nothing*
4	30 Jan 2009	< 12:00	08:00	nothing	nothing	nothing	nothing
8	15 Jul 2009	15:00	21:00	nothing	nothing	11:00, SE limb signature	nothing
9	31 Jul 2009	04:30	08:00	04:30	05:30	nothing	nothing*
10	25 Aug 2009	10:00	14:00	05:00	10:00	nothing	nothing
11	3 Sep 2009	08:00	21:24	< 02:00	08:45	Sep 2 16:15, limb signature, EP	nothing
12	25 Sep 2009	16:00	18:00	nothing	nothing	nothing	nothing
16	23 Oct 2009	< 16:00	not clearly visible	03:30	not clearly visible	02:00, dimming at limb	nothing
17	27 Oct 2009	17:00	17:00	15:30	10:30	nothing*	nothing*
19	6 Dec 2009	< 14:00	< 14:00	< 15:00	not clearly visible	nothing	nothing

[1] SE = southeast, EP = eruptive prominence.

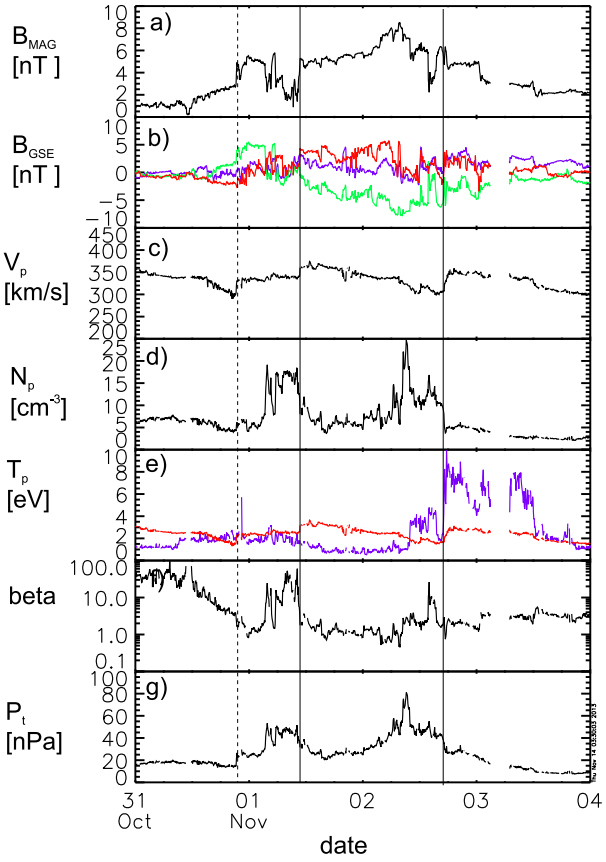

Figure 1 OMNI measurements during the ICME on 1 – 2 November 2009. The panels from top to bottom show (a) magnetic field magnitude, (b) magnetic field components in Geocentric Solar Ecliptic (GSE) coordinates (purple: B_X, green: B_Y, red: B_Z), (c) solar wind speed, (d) solar wind density, (e) temperature (purple: measured temperature, red: expected temperature, see text for details), (f) plasma β, and (g) perpendicular pressure (sum of the magnetic pressure and plasma thermal pressure perpendicular to the magnetic field). The ICME is bounded by a pair of solid lines and the dashed line marks the leading wave.

wave, observed on 31 October at 21:22 UT. magnetic field rotation occurs predominantly in the Y-component. The magnetic field is not particularly smooth, but this event is listed in the *Wind* magnetic-cloud list and the Lepping, Jones, and Burlaga (1990) flux rope fitting result is of fair quality (see the *Wind* list). Figure 1e shows the measured proton temperature [T_p; purple] and the expected solar wind temperature [T_{ex}; red], calculated from the empirical correlation between solar wind speed and proton temperature (Lopez, 1987). During the ICME T_p is below T_{exp}, which is a typical signature of ICME-related solar wind plasma according to Richardson and Cane (1995).

The estimated solar time for the ICME shown in Figure 1 was on 27 October at 6 UT. The upper panel of Figure 2 shows COR2 and LASCO/C3 images during the CME that was detected close to the estimated time. The first signatures of this CME in COR2 were observed on 27 October $\approx$ 17 UT. The CME had an AW of only 20°, but it was clearly seen by both STEREO spacecraft. However, nothing was detected in LASCO images. Figure 2 shows that the CME has a concave structure, which as mentioned in Section 2, outlines the bottom part of the flux rope cavity. However, no bright front is detected. The CME has a symmetric appearance in STEREO, and according to the FM analysis (see Figure 2 and Table 3), the CME propagation direction was at N03W06, *i.e.* the CME was heading directly towards Earth. Triangulation of the concave structure gives a similar propagation direction as the FM analysis, at N03W10. No other CME candidates were detected within the three-day time window around the estimated CME time.

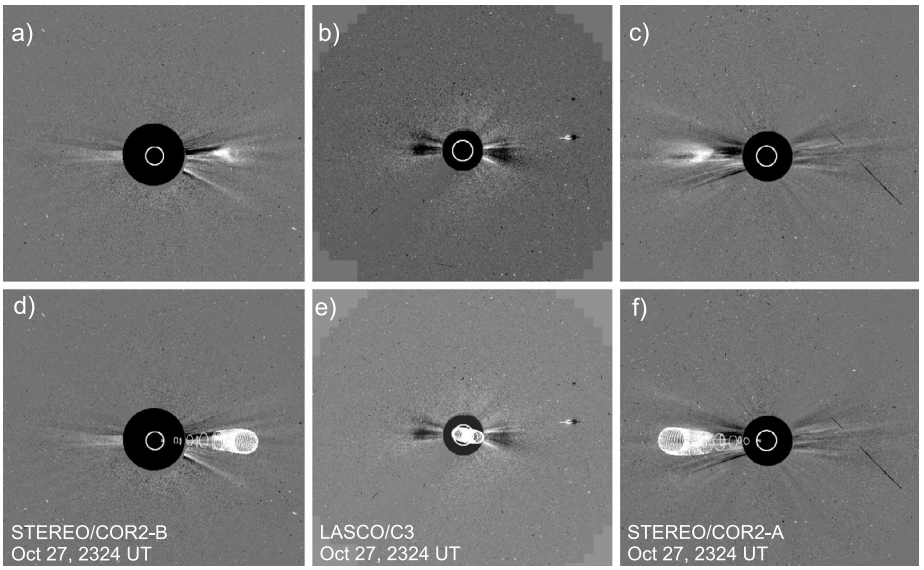

Figure 2 STEREO/COR2-B (left), STEREO/COR2-A (right) and LASCO-C3 (middle) coronagraph base-difference images on 27 October 2009 at 23:24 UT. The CME is seen only in STEREO-A and STEREO-B. Lower panels display the same images as the top panels, but the contours show the fit of the CME with the flux rope model (see Section 2).

As indicated in Table 4, the CME described above started very slowly; its first appearance in COR1-A is reported at 15:30 UT and in COR1-B at 10:30 UT. An EUV dimming associated with a small eruption occurred in Active Region (AR) 11029 located at N27W37 (Earth view) on 27 October around 8 UT. No other CME-related EUV signatures were detected. However, the dimming occurred relatively far from the CME apex as estimated by the FM analysis and triangulation (the difference in longitude was about 30°). For wide CMEs, relatively large differences in the source and CME apex longitudes may occur (*e.g.* Lara, 2008; Nieves-Chinchilla *et al.*, 2013) since EUV activity can be related to only one of the CME legs. Considering the narrow width of the 27 October CME (note that it is categorized as a narrow CME and not as a normal CME) and the reconstruction results, we do not consider it likely that the dimming was associated with the CME described above.

3.2. Example 2: 30 January – 4 February 2009

Figure 3 shows OMNI measurements during the ICME in early February 2009. The ICME drove a weak shock detected on 2 February at 20:16 UT. At the shock, the solar wind speed increased from about 300 to 350 km s^{-1}. The ICME started on 4 February at 1 UT and extended until 4 February at 18 UT. The ICME leading edge speed was 368 km s^{-1} and its duration was 17 hours. The maximum magnetic field magnitude during the ICME was 11.3 nT. The magnetic field had relatively large variations, and because of the relatively high density, the plasma β is only slightly lower than unity. However, the rotation of the magnetic field is clear, which suggests a flux rope structure. The P_t profiles show a rapid increase at the shock and then a plateau, suggesting that this flux rope was encountered at the intermediate distance from the center. Using the ICME leading edge speed, we estimate that the CME erupted on 30 January 7 UT. There were three CME candidates within the three-day time

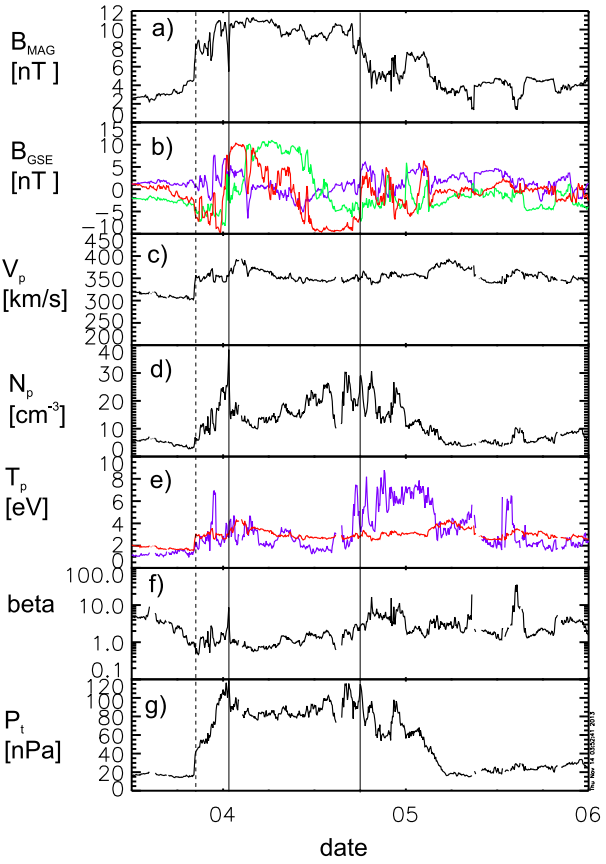

Figure 3 OMNI measurements during the ICME on 2 – 4 February 2009. The panels from top to bottom show (a) magnetic field magnitude, (b) magnetic field components in Geocentric Solar Ecliptic (GSE) coordinates (purple: B_X, green: B_Y, red: B_Z), (c) solar wind speed, (d) solar wind density, (e) temperature (purple: measured temperature, red: expected temperature, see text for details) (f) plasma β, and (g) perpendicular pressure (sum of the magnetic pressure and plasma thermal pressure perpendicular to the magnetic field). The dashed vertical line marks the shock, and the ICME is bounded by a pair of solid vertical lines.

window: i) 29 January (CME1), ii) 30 January (CME2), and iii) 31 January (CME3). The COR2-A and COR2-B running-difference snapshots of these CMEs are gathered in Figure 4.

CME1 (Figures 4a and 4b) was first detected in COR2-A on 29 January at 5 UT. In COR2-B, CME1 was hardly detectable. We did not find any EUV on-disk signatures, so this must have been a stealth CME. The AW of this CME was only $\approx 20°$ in COR2-A and $\approx 25°$ in COR2-B. Owing to the faintness of this CME, we could not perform FM. Triangulation gives the propagation direction towards S09E08. The CME was also so faint and unstructured in COR2-A that its speed could not be reliably measured. If CME1 was related to the ICME in question, its Sun-to-Earth travel time would have been at least 5.8 days (calculated from the first detection in COR2-A to the detection in the near-Earth solar wind). This gives an average transit speed of 299 km s^{-1}, which is quite slow when compared with the ICME leading edge speed (368 km s^{-1}).

CME2 (Figures 4c and 4d) appeared in COR2-A and COR2-B on 30 January ≈ 6 UT. CME2 was extremely faint at both STEREO spacecraft and no on-disk EUV activity was detected. The AW of CME2 was $\approx 55°$ in COR2-A and $\approx 50°$ in COR2-B. The speed measured from COR2-A was 300 km s^{-1} and from COR2-B 220 km s^{-1}. Because of the faintness of the event, we could not apply FM, but triangulation suggests that the CME was Earth-directed, with the propagation direction towards W03S02. While the running-difference images of CME2 displayed in Figure 4 show a fuzzy and unstructured appearance, the normal movies reveal that CME2 had an obviously concave structure. No bright outer rim was de-

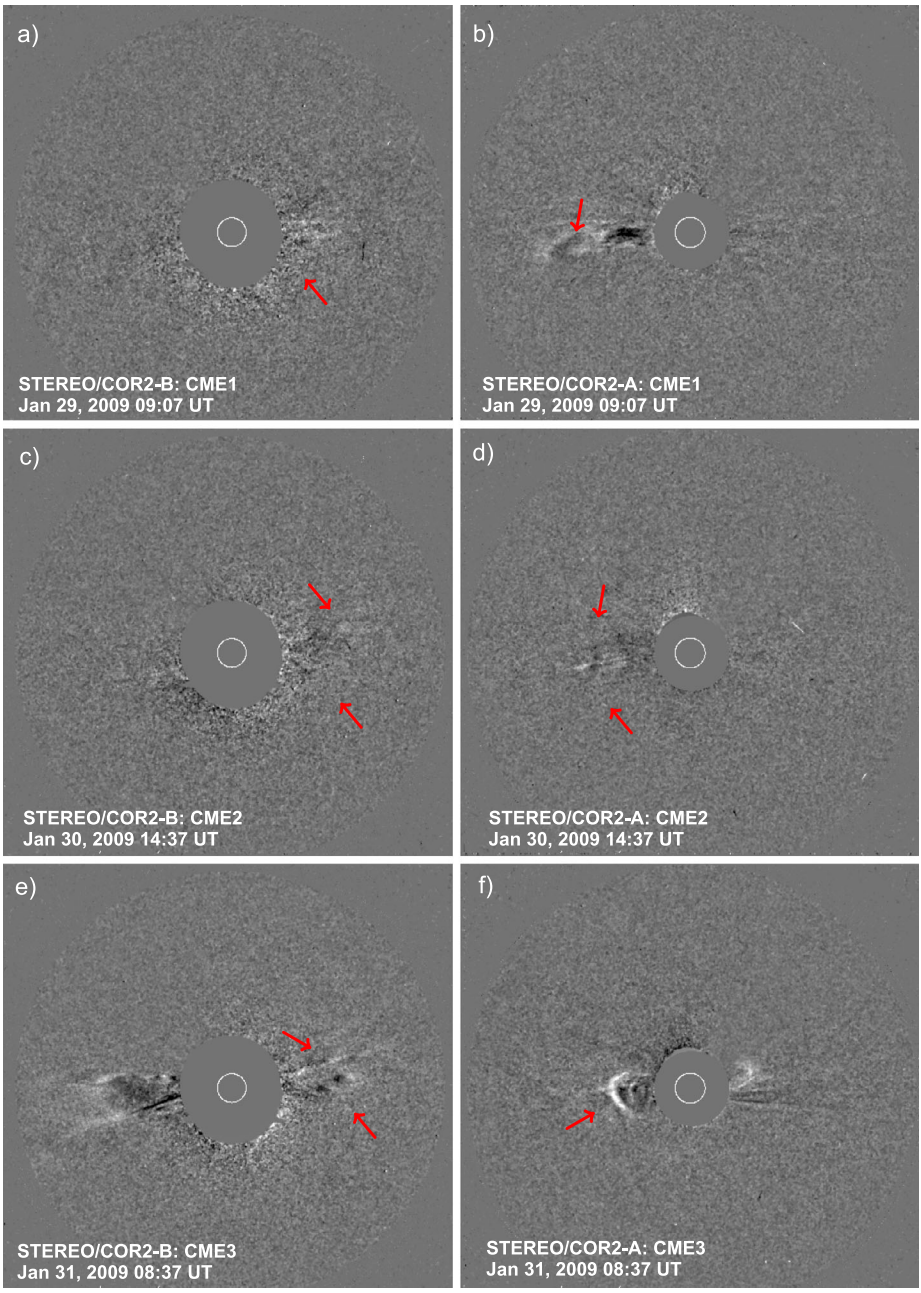

Figure 4 STEREO/COR2-B (left) and STEREO/COR2-A (right) running-difference images for three CMEs that were considered as the source for the 3 – 4 February ICME (Figure 3). (a) – (b) CME on 29 January 2009 at 09:07 UT, (c) – (d) CME on 30 January 2009 14:37 UT, and (e) – (f) CME on 31 January 08:37 UT.

tected. The Sun-to-Earth travel time for CME2 is 4.8 days, resulting in an average transit speed of 368 km s^{-1}, which exactly matches exactly the ICME leading edge speed.

CME3 (Figure 4e and 4f) was the brightest of the three CME candidates. CME3 was clearly seen in COR2-A where it first appeared on 31 January, 5 UT and had a three-part structure. CME3 was seen in COR2-B, but was much fainter and less structured than in COR2-A. Post-flare loops were detected after the CME launch. The AW of CME3 was $\approx 55^{\circ}$ in COR2-A, and its speed was 380 km s^{-1}. The Sun-to-Earth transit time of CME3 is 3.8 days, yielding an average transit speed of 455 km s^{-1}, which is considerably higher than the ICME leading edge speed. According to FM (results not shown), CME3 was heading somewhat away from the Sun-Earth-line (E21S13), suggesting only a glancing encounter with Earth.

Although CME3 was the brightest and most structured of the three candidates, based on the timing considerations and the propagation direction, CME2 seems the most likely candidate. The HI tracking is complex for this event, but it also supports a scenario in which the associated CME could have left the Sun on 30 January. The density front associated with the ICME on 2 – 4 February was seen in HI2-A and can be tracked backwards to HI1-A. The front enters HI1-A on 31 January at 8 UT, and is therefore not consistent with CME3 being the source. The tracking for this CME is difficult because the CME front catches up and merges with another front. This other front is probably associated with the on-going outflow activity from the nearby streamer.

4. Observations

4.1. Overview of ICMEs

We next describe the overall ICME properties listed in Table 1. The average values for $B_{\max}$, $V_{\max}$, and ΔT, as well as the number of centrally crossed ICMEs and FR-ICMEs are given in Table 5. The average $B_{\max}$ is 9.7 nT for all 20 ICMEs. In 2009 the interplanetary magnetic field (IMF) magnitude was remarkably weak and the solar wind speed was low (*e.g.* Jian, Russell, and Luhmann, 2011; Tsurutani, Echer, and Gonzalez, 2011; Kilpua *et al.*, 2013). The average IMF magnitude in 2009 was only 3.5 nT. All of our ICMEs had a $B_{\max}$ higher than this value, although as is seen from Table 1 two events (14, 15) had $B_{\max}$ only slightly higher than the average annual IMF magnitude. The strongest ICME in our data set had $B_{\max}$ of 18.6 nT (event 5). The average $V_{\max}$ within ICMEs was 354 km s^{-1}, slightly lower than the average solar wind speed in 2009 (364 km s^{-1}). It is noteworthy that all ICMEs in our data set were slow; the fastest ICME had $V_{\max}$ of only 439 km s^{-1} (20). The average ΔT for ICMEs was 20.1 hours. The ICMEs in 2009 had similar magnetic field magnitudes, but they were slightly slower and shorter than ICMEs reported during the previous solar-minimum year 1996. The mean $B_{\max}$, $V_{\max}$, and ΔT for the four ICMEs in 1996 included in the *Wind*, UCLA, and R&C lists were 9.3 nT, 393 km s^{-1}, and 28 hours, respectively.

Following Kilpua *et al.* (2011b), we used $B_{\max} = 7$ nT and ΔT ten hours to separate weak and significant ICMEs. Significant ICMEs were required to have $B_{\max} \geq 7$ nT and $\Delta T \geq$ ten hours. Using this definition, our data set includes 12 (60 %) significant ICMEs and eight (40 %) weak ICMEs. Table 5 shows the average properties for weak and significant ICMEs separately.

Sixteen events were in the P_{t} category. Table 5 shows that eight ICMEs were crossed centrally (Group 1), six were crossed from the intermediate distances from the center (Group 2), and two close to the edge (Group 3). The four ICMEs that do not fall into the P_{t} category

Table 5 ICME properties. The first row gives the statistics for all 20 ICMEs in this study. The next two rows give the statistics for weak and significant ICMEs separately (see Section 4.1). The last two rows give the statistics for ICMEs associated with stealth and non-stealth CMEs separately.

	Event	$\langle \Delta T \rangle$[1] [hours]	$\langle B_{\max} \rangle$[2] [nT]	$\langle V_{\max} \rangle$[3] [km s^{-1}]	P_t Group 1[4]	FR-ICME[5]
All ICMEs	20	20.1 ± 9.9	9.7 ± 4.0	354 ± 40	8/16 (50 %)	12 (60 %)
Significant ICMEs	12	23.8 ± 7.9	10.8 ± 3.4	346 ± 34	5/9 (56 %)	8 (67 %)
Weak ICMEs	8	14.5 ± 9.7	7.3 ± 3.7	365 ± 48	3/7 (43 %)	4 (50 %)
Stealth CMEs	10	20.2 ± 8.8	9.7 ± 3.1	345 ± 36	4/7 (57 %)	7 (70 %)
Non-stealth CMEs	6	21.5 ± 10.5	8.15 ± 3.7	361 ± 52	1/5 (20 %)	3 (50 %)

[1]The average ICME duration.

[2]The average peak magnetic field with the ICME.

[3]The average maximum speed within the ICME.

[4]The number of centrally encountered ICMEs from the subset for which the perpendicular pressure group was determined.

[5]The number of flux rope-type ICMEs.

were all trailed by a high-speed solar wind stream. Table 5 also shows that significant ICMEs were crossed slightly more often centrally than weak ICMEs.

Table 5 shows that 12 out of 20 (60 %) ICMEs had an FR structure. Of eight complex (non-FR) ICMEs, two were centrally crossed, two were crossed from an intermediate distance from the center, and two far from the center. In turn, six FR-ICMEs were encountered centrally. Half of the weak ICMEs were flux ropes, while the percentage of flux rope-type significant ICMEs was slightly higher (67 %).

The last two panels of Table 1 give the minimum Dst and maximum Kp indices associated with ICMEs. We have shown these values only if the Dst minimum was ≤ -30 nT and if the Kp maximum was at least 4–. Most ICMEs in 2009 did not cause significant geomagnetic activity. For six ICMEs the Kp storm limit was exceeded, and for three ICMEs, Dst decreased below -30 nT. The strongest Kp storms (Kp = 6) occurred on 21 July 2009 (Event 8) and on 30 August 2009 (Event 10). Both of the ICMEs were interacting with the trailing high-speed stream. For the latter case, Dst did not exceed the storm limit, but for the former case, a moderate Dst storm ensued with a lowest value of -83 nT (strongest Dst storm in this data set).

4.2. White-Light CME Associations

4.2.1. CME Associations and Their Properties

We were able to find white-light associations for 16 out of 20 (80 %) ICMEs. Three events (12, 15, 17) had AW $\leq 20^\circ$ and can therefore be considered narrow CMEs (*e.g.* Yashiro *et al.*, 2003; Mittal *et al.*, 2009). The average properties for CMEs are given in Table 6. The average AW for CMEs (AW $> 20^\circ$) was around 47°. This coincides with AW of 47° in 1996 reported by Yashiro *et al.* (2004) (note that in Yashiro *et al.* (2004) all CMEs with $20^\circ <$ AW $\leq 120^\circ$ were considered, not just those that impacted Earth). The mean speed in our data set was 321 km s^{-1} for CMEs with AW $> 20^\circ$ and 307 km s^{-1} for narrow CMEs. The highest speed, 520 km s^{-1}, was measured for Event 20.

Table 6 CME properties. The first row show the statistics for CMEs with angular width $> 20°$ and the second row for narrow CMEs (angular width $\leq 20°$). The last two rows compare the properties of stealth and non-stealth CMEs for which the angular width was $> 20°$.

	Events	⟨AW⟩[1] [°]	⟨Speed⟩[2] [km s^{-1}]	FR-CME[3]	Bright front[4]
CMEs (AW $> 20°$)	13	47 ± 14	321 ± 103	11 (85 %)	6 (38 %)
narrow CMEs	3	16 ± 4	307 ± 91	1 (33 %)	0 (0 %)
stealth CMEs (AW $> 20°$)	8	41 ± 11	288 ± 84	6 (75 %)	1 (13 %)
non-stealth CMEs (AW $> 20°$)	5	55 ± 17	376 ± 130	5 (100 %)	5 (100 %)

[1]CME average angular width as measured in COR2.

[2]CME average speed measured in COR2.

[3]The number of CMEs with flux rope morphology.

[4]The number of events for which a bright front was identified in coronagraph images/movies.

In only six cases did LASCO detect the CME. The AW of these CMEs as reported in the LASCO catalog are given in Table 2. The obvious reason for the lack of LASCO detection is that the analyzed CMEs were in general faint and narrow, and because they headed more or less directly towards LASCO, they were not detected because they were hidden by the occulter (see Section 2). In three cases (Events 2, 3, and 10) the same CME that was deteced in the near-Earth solar wind was also detected by one of the STEREO spacecraft. In one case (Event 20) the ICME was encountered far from the center (P_t category 3). According to the FM analysis, the CME on 23 June 2009 was propagating away from the Sun–Earth line (W19S09). For the associated ICME the P_t category could not be defined. For Event 16 there was a substantial data gap in STEREO observations, and therefore no FM analysis could be performed to determine the CME propagation direction. Thus, at least in five of these cases the CME had a clear component off the Sun–Earth line. It is interesting to note that only one of the CMEs captured by LASCO was a halo CME (Event 20). All of the other five CMEs had an AW $< 120°$, *i.e.* they were narrower than the partial-halo limit.

The column "Type" in Table 2 gives information on the CME white-light morphology. Twelve out of 16 (75 %) CME associations showed flux rope signatures (see Section 2) and are labeled as "FR" in Table 2. Four CMEs without flux rope signatures in coronagraph images are marked as "flows". All flow-like CMEs had AW $< 30°$. However, note that the narrow CME on 27 October 2009 showed flux rope signatures (clear concave structure; see Figure 2).

We confirmed for ten FR-CMEs using the FM analysis and for four flow-like CMEs using triangulation that they were directed towards the Earth (see Section 2 and Table 3). The HI tracking confirmed the arrival at Earth for ten FR-CMEs. All flow-like CMEs were too faint to be followed in HI. For the CME on 23 October 2009 (Event 17) the FM and HI tracking could not be performed because of a substantial data gap in STEREO (only the early evolution of the CME was seen in COR2). Additionally, the CME on 31 July 2009 could not be followed by HI because this CME was entrained by a SIR. However, according to the FM analysis, this CME was Earth-directed. The ICME on 30 August 2009 and the associated CME on 25 August (Event 10) were discussed extensively by Nieves-Chinchilla *et al.* (2013). The CME was part of a double eruption of an extended filament channel. The first part of the eruption arrived at STEREO-B, while the second part arrived at Earth.

4.2.2. ICMEs Without White-Light Association

The lack of a white-light counterpart for the ICME on 11 – 12 March 2009 (Event 5), the strongest ICME in our data set, is most likely related to the substantial STEREO data gap (in STEREO-A during 6 March, 7 – 18 UT and 7 March, 2 – 19 UT, in STEREO-B during 6 March 2 – 20 UT). For the ICME detected on 3 – 4 June 2009 we could not find any Earth-directed CMEs. Two CMEs occurred within a suitable time window. However, the first of these on 29 May impacted STEREO-A (with no apparent Earth-directed component), and the second, early on 30 May, was not Earth-directed either based on its appearance in coronagraph images or according to the FM analysis. It is possible that these relatively bright CMEs have obscured some fainter and narrower Earth-directed CMEs. However, no activity was detected in EUV close to the disk center. The 2 – 4 June ICME had $B_{\max}$ of 7.0 nT and duration of 38 hours. The P_{t} profile suggested an encounter close to the edge. However, there are no indications in HI that the 29 May CME would have been deflected during its interplanetary travel towards Earth.

The remaining two ICMEs without CME associations were weak ICMEs observed in the near-Earth solar wind on 12 – 13 October 2009 (Event 13) and on 16 – 17 October 2009 (Event 14). According to the P_{t} profile, both of them were encountered centrally, suggesting that they were caused by intrinsically weak CMEs and were not an edge of stronger CMEs. Therefore it is possible that the associated eruptions were too weak and narrow to leave any discernible trace in white light. In addition, the weak ICME on 17 – 18 October 2009 (Event 15) that had a $B_{\max}$ of only 3.7 nT was associated with a very faint and flow-type narrow CME.

4.2.3. Comparison of CME and ICME Properties

Only half of the 12 FR-CMEs were associated with an FR-ICME. Of the six complex ICMEs that were related to FR-CMEs, three were crossed away from the center, and in two cases we could not define the impact parameter because the ICME was interacting with a high-speed stream. Interestingly, all flow-like CMEs were associated with an FR-ICME. One such example is shown in Figures 5 and 6. Figure 5 shows that the magnetic field rotates coherently within the ICME and that the proton temperature is low. The ICME was trailed by a high-speed stream that strongly compressed the rear portion of the ICME. This makes the P_{t} profile difficult to interpret, but an extended plateau suggests that the ICME was encountered from an intermediate distance from its center. The associated CME entered the COR2-A field of view on 15 July 22 UT and had AW 28°. Figure 6 shows that the CME had an unstructured, flow-like appearance with a ragged front. Triangulation gives the propagation direction towards E02N04. In COR2-B the CME was very faint, and LASCO did not observe any signatures of this CME. No other CME candidates were identified within a suitable time window.

As mentioned in Section 4.1, our study includes eight weak ICMEs. Two of them did not have any white-light counterpart (Events 13 and 14, see Section 4.2.2), one (Event 15) was associated with a narrow CME, and one (Event 1) with a flow-like CME with an AW of only 26°. The four remaining weak ICMEs (Events 2, 10, 11, and 20) were edge encounters of larger CMEs.

4.3. EUV and White-Light Signatures

The two last columns in Table 2 give information on the identified on-disk EUV activity. Of the total of 16 CMEs, ten (63 %) were stealth events, *i.e.* we did not observe on-disk EUV

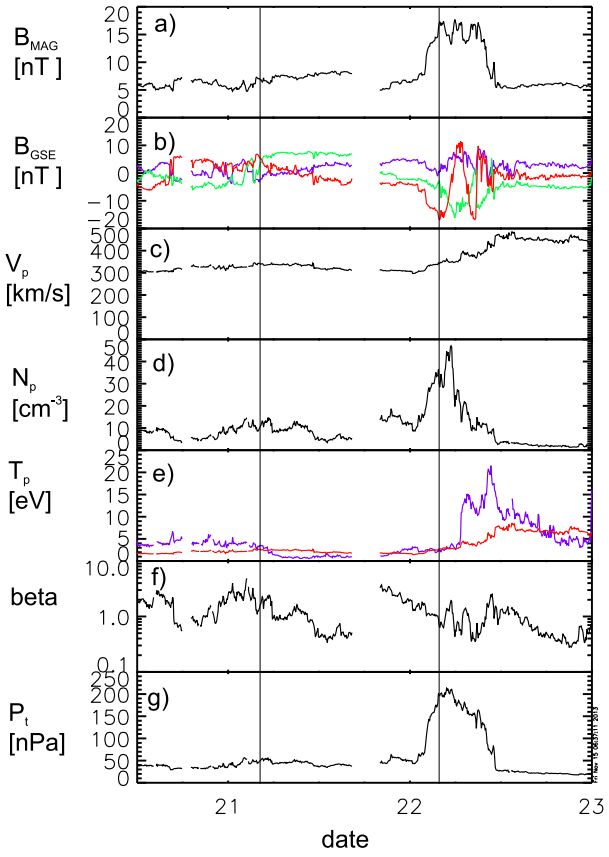

Figure 5 OMNI measurements during the ICME on July 21 – 22 2009. The panels from top to bottom show (a) magnetic field magnitude, (b) magnetic field components in Geocentric Solar Ecliptic (GSE) coordinates (purple: B_X, green: B_Y, red: B_Z), (c) solar wind speed, (d) solar wind density, (e) temperature (purple: measured temperature, red: expected temperature, see text for details) (f) plasma β, and (g) perpendicular pressure (sum of the magnetic pressure and plasma thermal pressure perpendicular to the magnetic field). The ICME is bounded by a pair of vertical solid lines.

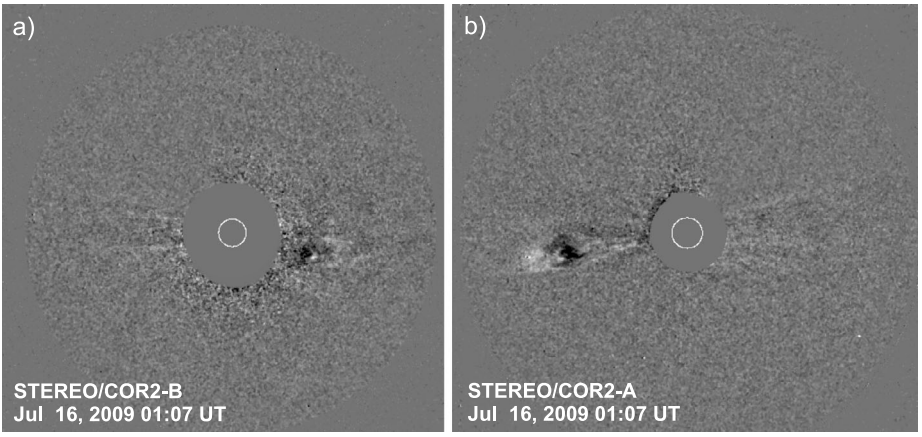

Figure 6 STEREO/COR2-B (left) and STEREO/COR2-A (right) running-difference images on 16 July 2009 at 01:07 UT featuring the CME associated with the ICME shown in Figure 5.

signatures. From 13 CMEs with AW $> 20^{\circ}$ eight (62 %) were stealth, while two out of the three narrow CMEs were stealth CMEs.

Table 4 presents the results of the more detailed analysis of stealth CMEs and their low-corona signatures (for the procedure, see Section 2). The first appearance in the two COR1 and COR2 fields of view is given. The times are approximate because the events were slow and faint or occurred close in time to previous flows. The events marked with an asterisk in either of the last two columns of Table 4 are those for which a tentative source region was found in EUVI images but its position did not correspond to the CME appearance in the coronagraph field of view (FOV). For example, the CME on 31 July 2009 appears first in the COR2-A FOV and it is brighter than the same CME seen by COR2-B, which has the appearance of a partial-halo CME. This suggests that the CME is coming from a region close to the limb in STEREO-A observations and from the disk as seen by STEREO-B. However, the only low-corona phenomenon possibly associated with this CME (small-scale loop opening) is situated above the limb as seen by STEREO-B. The discrepancy between this tentative source region at the limb and the partial-halo appearance indicates that the low-corona source was not identified correctly and this loop opening is not associated with the CME. Therefore, we wrote "nothing" in the corresponding column of Table 4, as for other stealth CMEs.

The average properties of stealth and non-stealth CMEs are shown in Table 6. Stealth CMEs were on average narrower and slower than the CMEs related to on-disk EUV activity: the mean AW for stealth CMEs was 41° and for non-stealth CMEs 55°. The mean speeds (in COR2) were 288 km s^{-1} and 376 km s^{-1} for stealth and non-stealth CMEs. EUV dimming was the most typical activity that we could discern from the EUV movies. Only two CMEs (Events 7 and 20) originated from an active region, and only one event in our data set was associated with a flare (C5 class flare related to the 16 December 2009 CME).

Table 6 also shows that all except one stealth CMEs lacked the leading bright front in coronagraphic images. In turn, for all non-stealth CMEs we identified the bright loop. Therefore, stealth CMEs were identified from coronagraphic data based on the observation of a concave structure, which, as explained in Section 2, features the lower part of the flux rope cavity (see also example presented in Section 3.2).

Next, we compare the average properties of ICMEs related to stealth and non-stealth CMEs. The average $B_{\max}$, $V_{\max}$, and ΔT for ICMEs related to stealth and non-stealth CMEs are given in Table 5. ICMEs associated with stealth CMEs had, in general, higher $B_{\max}$, similar durations, and slightly lower speeds than ICMEs related to non-stealth CMEs. In addition, a significantly larger percentage of stealth CMEs were associated with FR-type ICMEs than non-stealth CMEs. This result might be biased by the impact parameter: as shown in Table 5, ICMEs related to stealth CMEs were crossed centrally more often than ICMEs related to non-stealth CMEs.

5. Discussion and Conclusions

In this article we have searched for and analyzed the solar counterparts for 20 solar-minimum ICMEs. The investigated period is the year 2009, which coincides with the deep solar minimum between Solar Cycles 23 and 24. In 2009, the two STEREO spacecraft were ideally located to observe Earth-directed CMEs.

After a careful inspection of coronagraph movies and with the aid of forward modeling, triangulation, and HI tracking, we found white-light counterparts for 16 (80 %) ICMEs. For two cases the lack of CME association is likely attributable to a data gap or to a brighter

CME that obscured a fainter Earth-directed CME. For the other two cases no coherent outflows or CMEs were detected within a suitable temporal window.

Our study showed that the wide-angle view point from STEREO is crucial to detect solar counterparts for weak ICMEs during solar-activity minimum. LASCO detected the CME for only six ICMEs in our data set. At least five of these CMEs had a significant off-Earth component, and all except one CME were relatively narrow in the LASCO view (smaller than the partial-halo CME limit of 120°). This shows that a full or partial-halo CME observation is not necessary to observe a CME arrival.

It was somewhat surprising that even with the off-angle view offered by STEREO we had difficulties finding the white-light counterpart for several ICMEs. During solar minimum, CME activity is clearly lower than at activity maximum (*e.g.* Yashiro *et al.*, 2004; Gopalswamy, 2006), but blobs and narrow and/or faint CMEs are observed on a daily basis. As shown by our example event (Section 3.2), a careful inspection of coronagraph movies, timing considerations, and support from CME reconstruction methods and white-light tracking are needed to make the correct association. The STEREO configuration also allowed us to show that narrow CMEs (AW $\leq 20°$) can arrive at Earth and exhibit clear *in-situ* signatures. None of the narrow CMEs that arrived at Earth were detected by LASCO.

In addition, many CMEs were extremely faint in the coronagraphic data and did not leave obvious traces on the solar disk. In our study 10 out of 16 (63 %) CMEs were stealth CMEs. Furthermore, only two of our stealth CMEs showed variations in EUV when viewed above the limb (however, most of them were detected in COR1). Stealth CMEs without EUV limb signatures have been reported in previous studies, for example by Ma *et al.* (2010), who found EUV limb signatures for more than half of their stealth CMEs. All except one stealth CME in our study lacked the bright front in coronagraphic data, while all non-stealth CMEs showed this structure. Consequently, stealth CMEs were identified based on the concave structure, which as discussed in Section 2 outlines the bottom part of the flux rope cavity. Our results are consistent with the conclusions of Robbrecht, Patsourakos, and Vourlidas (2009) and Ma *et al.* (2010) that stealth CMEs start slower and form at higher coronal altitudes than non-stealth CMEs. We suggest that weak CMEs that form at relatively high altitudes in the corona, and in particular accelerate slowly, may not gather enough coronal plasma at the front edge of the flux rope to form the bright front. The lack of EUV-limb signatures may be related to higher formation altitude, where the lower densities will result in weak EUV emission in the EUVI passbands. On the other hand, the wide passband of COR1 was able to detect these CMEs in most cases.

Stealth CMEs without a frontal rim and with only a faint bottom part are difficult to detect even when viewed from the side, particularly when they also lack on-limb signatures. It is possible that two weak ICMEs for which we could not find the white-light counterpart were caused by such stealth CMEs (note also that for our example event in Section 3.2 the correct CME association was very difficult to make because of the lack of the frontal rim and very faint bottom part). The lack of a bright front may also complicate the determination of CME parameters, in particular the CME speed, which is usually calculated as the speed of the front loop. Stealth CMEs may be partly responsible for the differences between CME and ICME rates (*e.g.* Riley *et al.*, 2006; Kilpua *et al.*, 2011a,b), in particular during low solar activity when stealth CMEs seem to be common, as reported by Ma *et al.* (2010). Stealth CMEs have not yet been studied in a systematic way in solar-maximum conditions.

According to our study, there is no intrinsic difference in ICMEs associated with stealth and non-stealth CMEs. The clearest discrepancy was in the fraction of flux rope-type ICMEs, but this can probably be attributed to the fact that in our data set events associated with stealth CMEs were crossed more often centrally than ICMEs associated with non-stealth CMEs. Thus, a larger data set is needed to study these issues. As expected, stealth

CMEs were somewhat slower and narrower than non-stealth CMEs. It is also an interesting question whether release mechanisms are different for stealth and non-stealth CMEs or are the only significant differences the speed of their early coronal development and the altitude of their origin. For example, post-flare loops are an intrinsic consequence of the break-out model (*e.g.* Antiochos, DeVore, and Klimchuk, 1999), where reconnection occurs both above and below the erupting structure. If this mechanism applies to stealth CMEs, the reconnection must occur slowly and high in the corona, resulting in much reduced heating as explained by Robbrecht, Patsourakos, and Vourlidas (2009).

Our study showed that CMEs with flux rope morphology can result in complex ICMEs, and unstructured CMEs can result in flux rope ICMEs (see example in Section 4.2.3). The former connection is supported by several previous studies (*e.g.* Cane, Richardson, and Wibberenz, 1997; Jian *et al.*, 2006; Dasso *et al.*, 2007; Kilpua *et al.*, 2011c; Mohamed *et al.*, 2012), suggesting that complex ICMEs are associated with edge encounters of flux ropes or distorted flux ropes. This was also the case in our study; complex ICMEs were more frequently associated with larger impact parameters than flux rope ICMEs. Connecting an unstructured CME with a flux rope-type ICME is an interesting result considering the open question in the field whether all CMEs are intrinsically flux ropes (*e.g.* Vourlidas *et al.*, 2013). Our results are consistent with the results of Sheeley *et al.* (2009) (see also discussion by Vourlidas *et al.*, 2013) that the flux rope visibility in coronagraphic data depends on the viewing angle.

Finally, although solar-minimum ICMEs are important in many aspects (see Section 1), they are rarely geoeffective. The two strongest geomagnetic storms related to ICMEs in our data set were moderate storms caused by an ICME interacting with the trailing SIR. Thus, stealth CMEs may act an "enhancers" of the geoeffectiveness of SIRs by adding an additional component of magnetic field in the SIR–magnetosphere interaction. In one of these cases the ICME was associated with a faint and narrow unstructured flow-type stealth CME, which was difficult to detect even by STEREO. Thus, no prior warning could have been provided.

Acknowledgements The LASCO CME catalog is generated and maintained at the CDAW Data Center by NASA and The Catholic University of America in cooperation with the Naval Research Laboratory. SOHO is a project of international cooperation between ESA and NASA. The authors thank the STEREO/SECCHI consortium for providing the data. The SECCHI data used here were produced by an international consortium of the Naval Research Laboratory (USA), Lockheed Martin Solar and Astrophysics Lab (USA), NASA Goddard Space Flight Center (USA), Rutherford Appleton Laboratory (UK), University of Birmingham (UK), Max-Planck-Institut for Solar System Research (Germany), Centre Spatiale de Liège (Belgium), Institut d'Optique Theorique et Appliquée (France), and Institut d'Astrophysique Spatiale (France). LR partially contributes to the research for the European Union Seventh Framework Programme (FP7/2007-2013) under grant agreement number 263252 [COMESEP]. We acknowledge support from the Belgian Federal Science Policy Office (BELSPO) through the ESA-PRODEX program. We acknowledge support from the CHARM framework (Contemporary physical challenges in Heliospheric and AstRophysical Models), a phase VII Interuniversity Attraction Pole (IAP) program organised by BELSPO. This research has been funded by the Interuniversity Attraction Poles Programme initiated by the Belgian Science Policy Office (IAP P7/08 CHARM). EKJK acknowledges the Academy of Finland (project 1218152). MM would like to thank Eva Robbrecht and Elke D'Huys for constructive discussions on stealth CMEs.

References

Antiochos, S.K., DeVore, C.R., Klimchuk, J.A.: 1999, A model for solar coronal mass ejections. *Astrophys. J.* **510**, 485. DOI.

Brueckner, G.E., Howard, R.A., Koomen, M.J., Korendyke, C.M., Michels, D.J., Moses, J.D.: 1995, The Large Angle Spectroscopic Coronagraph. *Solar Phys.* **162**, 357. DOI.

Cane, H.V.: 2000, Coronal mass ejections and Forbush decreases. *Space Sci. Rev.* **93**, 55.
Cane, H.V., Richardson, I.G., Wibberenz, G.: 1997, Helios 1 and 2 observations of particle decreases, ejecta, and magnetic clouds. *J. Geophys. Res.* **102**(A4), 7075. DOI.
Chen, J., Howard, R.A., Brueckner, G.E., Santoro, R., Krall, J., Paswaters, S.E., St. Cyr, O.C., Schwenn, R., Lamy, P., Simnett, G.M.: 1997, Evidence of an erupting magnetic flux rope: LASCO coronal mass ejection of 1997 April 13. *Astrophys. J. Lett.* **490**, L191. DOI.
Dasso, S., Nakwacki, M.S., Demoulin, P., Mandrini, C.H.: 2007, Progressive transformation of a flux rope to an ICME. Comparative analysis using the direct and fitted expansion methods. *Solar Phys.* **244**, 115. DOI.
Delaboudiniére, J.-P., Artzner, G.E., Brunaud, J., Gabriel, A.H., Hochedez, J.F., Millier, F., Song, X.Y., Au, B., Dere, K.P., Howard, R.A., Kreplin, R., Michels, D.J., Moses, J.D., Defise, J.M., Jamar, C., Rochus, P., Chauvineau, J.P., Marioge, J.P., Catura, R.C., Lemen, J.R., Shing, L., Stern, R.A., Gurman, J.B., Neupert, W.M., Maucherat, A., Clette, F., Cugnon, P., Dessel, E.L.: 1995, EIT: Extreme-ultraviolet Imaging Telescope for the SOHO mission. *Solar Phys.* **162**, 291. DOI.
Eyles, C.J., Simnett, G.M., Cooke, M.P., Jackson, B.V., Buffington, A., Hick, P.P., Waltham, N.R., King, J.M., Anderson, P.A., Holladay, P.E.: 2003, The Solar Mass Ejection Imager (SMEI). *Solar Phys.* **217**, 319. DOI.
Feng, H.Q., Wu, D.J., Lin, C.C., Chao, J.K., Lee, L.C., Lyu, L.H.: 2008, Interplanetary small- and intermediate-sized magnetic flux ropes during 1995 – 2005. *J. Geophys. Res.* **113**, A12105. DOI.
Gomez-Herrero, R., Malandraki, O.E., Dresing, N., Kilpua, K., Heber, B., Klassen, A., Muller-Mellin, R., Wimmer-Schweingruber, R.F.: 2011, Spatial and temporal variations of CIRs: multi-point observations by STEREO. *J. Atmos. Solar-Terr. Phys.* **73**, 551. DOI.
Gopalswamy, N.: 2006, Coronal mass ejections of cycle 23. *J. Astrophys. Astron.* **27**, 243.
Gosling, J.T.: 1997, In: Crooker, N., Joselyn, J.A., Feynman, J. (eds.) *Coronal Mass Ejections*, *Geophys. Monogr.* **99**, AGU, Washington, 245.
Gosling, J.T., McComas, D.J., Phillips, J.L., Bame, S.J.: 1991, Geomagnetic activity associated with earth passage of interplanetary shock disturbances and coronal mass ejections. *J. Geophys. Res.* **96**, 7831.
Gurman, J.B., Thompson, B.J., Newmark, J.A., Deforest Craig, E.: 1998, New images of the solar corona. In: Donahue, R.A., Bookbinder, J.A. (eds.) *The Tenth Cambridge Workshop on Cool Stars, Stellar Systems and the Sun*, **CS-154**, Astron. Soc. Pacific, San Francisco, 329.
Harrison, R.A., Davis, C.J., Eyles, C.J.: 2005, The STEREO heliospheric imager: how to detect CMEs in the heliosphere. *Adv. Space Res.* **36**, 1512. DOI.
Harrison, R.A., Davies, J.A., Rouillard, A.P., Davis, C.J., Eyles, C.J., Bewsher, D., Crothers, S.R., Howard, R.A., Sheeley, N.R., Vourlidas, A., Webb, D.F., Brown, D.S., Dorrian, G.D.: 2009, Two years of the STEREO heliospheric imagers. *Solar Phys.* **256**, 219. DOI.
Howard, R.A., Michels, D.J., Sheeley, N.R. Jr., Koomen, M.J.: 1982, The observation of a coronal transient directed at earth. *Astrophys. J.* **263**, L101. DOI.
Howard, T.A., Nandy, D., Koepke, A.C.: 2008a, Kinematic properties of solar coronal mass ejections: correction for projection effects in spacecraft coronagraph measurements. *J. Geophys. Res.* **113**, A01104. DOI.
Howard, R.A., Moses, J.D., Vourlidas, A., Newmark, J.S., Socker, D.G., Plunkett, S.P., Korendyke, C.M., Cook, J.W., Hurley, A., Davila, J.M., Thompson, W.T., St. Cyr, O.C., Mentzell, E., Mehalick, K., Lemen, J.R., Wuelser, J.P., Duncan, D.W., Tarbell, T.D., Wolfson, C.J., Moore, A., Harrison, R.A., Waltham, N.R., Lang, J., Davis, C.J., Eyles, C.J., Mapson-Menard, H., Simnett, G.M., Halain, J.P., Dese, J.M., Mazy, E., Rochus, P., Mercier, R., Ravet, M.F., Delmotte, F., Auchere, F., Delaboudiniere, J.P., Bothmer, V., Deutsch, W., Wang, D., Rich, N., Cooper, S., Stephens, V., Maahs, G., Baugh, R., Mc-Mullin, D., Carter, T.: 2008b, Sun Earth Connection Coronal and Heliospheric Investigation (SECCHI). *Space Sci. Rev.* **36**, 67. DOI.
Hudson, H.S., Cliver, E.W.: 2001, *J. Geophys. Res.* **106**, 25199. DOI.
Hundhausen, A.J.: 1993, Sizes and locations of coronal mass ejections – SMM observations from 1980 and 1984 – 1989. *J. Geophys. Res.* **98**, 13177. DOI.
Hundhausen, A.J., Sawyer, C.B., House, L., Illing, R.M.E., Wagner, W.J.: 1984, Coronal mass ejections observed during the solar maximum mission – latitude distribution and rate of occurrence. *J. Geophys. Res.* **89**, 2639. DOI.
Huttunen, K.E.J., Koskinen, H.E.J., Schwenn, R.: 2002, Variability of magnetospheric storms driven by different solar wind perturbations. *J. Geophys. Res.* **107**, 1121. DOI.
Illing, R.M.E., Hundhausen, A.J.: 1985, Observation of a coronal transient from 1.2 to 6 solar radii. *J. Geophys. Res.* **90**, 275. DOI.
Inhester, B.: 2006, Stereoscopy basics for the STEREO mission. arXiv.
Innes, D.E., Genetelli, A., Attie, R., Potts, H.E.: 2009, Quiet Sun mini-coronal mass ejections activated by supergranular flows. *Astron. Astrophys.* **495**, 319. DOI.

Jian, L., Russell, C.T., Luhmann, J.G.: 2011, Comparing solar minimum 23/24 with Historical solar wind records at 1 AU. *Solar Phys.* DOI.

Jian, L., Russell, C.T., Luhmann, J.G., Skoug, R.M.: 2006, Properties of interplanetary coronal mass ejections at one AU during 1995. *Solar Phys.* **239**, 393. 2004. DOI.

Kaiser, M., Kucera, T.A., Davila, J.M., St. Cyr, O.C., Guhathakurta, M., Christian, E.: 2007, The STEREO mission: an introduction. *Space Sci. Rev.* **135**, 5. DOI.

Kilpua, E.K.J., Pomoell, J., Vourlidas, A., Vainio, R., Luhmann, J., Li, Y., Schroeder, P., Galvin, A.B., Simunac, K.: 2009, STEREO observations of interplanetary coronal mass ejections and prominence deflection during solar minimum period. *Ann. Geophys.* **27**, 4491. DOI.

Kilpua, E.K.J., Lee, C.O., Luhmann, J.G., Li, Y.: 2011a, Interplanetary coronal mass ejections in the near–Earth solar wind during the minimum periods following solar cycles 22 and 23. *Ann. Geophys.* **29**, 1455. DOI.

Kilpua, E.K.J., Lian, J.K., Li, Y., Luhmann, J.G., Russell, C.T.: 2011b, Observations of ICMEs and ICME-like structures between 2007 – 2010 using near-Earth and STEREO observations. *Solar Phys.* **281**, 391. DOI.

Kilpua, E.K.J., Lian, J.K., Li, Y., Luhmann, J.G., Russell, C.T.: 2011c, Multipoint ICME Encounters: Pre-STEREO and STEREO Observations. *J. Atmos. Solar-Terr. Phys.* **73**, 1228. DOI.

Kilpua, E.K.J., Mierla, M., Rodriguez, L., Zhukov, A.N., Srivastava, N., West, M.J.: 2012, Estimating travel times of coronal mass ejections to 1 AU using multi-spacecraft coronagraph data. *Solar Phys.* **279**, 477. DOI.

Kilpua, E.K.J., Luhmann, J.G., Jian, L.K., Russell, C.T., Li, Y.: 2013, Why have geomagnetic storms been so weak during the recent solar minimum and the rising phase of cycle 24? *J. Atmos. Solar-Terr. Phys.* **107**, 12.

Lara, A.: 2008, The source region of coronal mass ejections. *Astrophys. J.* **688**, 647. DOI.

Lepping, R.P., Jones, J.A., Burlaga, L.F.: 1990, Magnetic field structure of interplanetary magnetic clouds at 1 AU. *J. Geophys. Res.* **95**, 11,957.

Lepping, R.P., Wu, C.-C.: 2010, Selection effects in identifying magnetic clouds and the importance of the closest approach parameter. *Ann. Geophys.* **28**, 1539. DOI.

Lopez, R.E.: 1987, Solar cycle invariance in solar wind proton temperature relationships. *J. Geophys. Res.* **92**, 11189. DOI.

Lugaz, N., Manchester, W.B., Gombosi, T.I.: 2005, The evolution of coronal mass ejection density structures. *Astrophys. J.* **627**, 1019.

Ma, S., Attril, G.D.R., Golub, L., Lin, J.: 2010, Statistical study of coronal mass ejections with and without distinct low coronal signatures. *Astrophys. J.* **722**, 289.

Mittal, N., Pandey, K., Narain, U., Sharma, S.S.: 2009, On properties of narrow CMEs observed with SOHO/LASCO. *Astrophys. Space Sci.* **323**, 135.

Mohamed, A.A., Gopalswamy, N., Yashiro, S., Akiyama, S., Mäkelä, P., Xie, H., Jung, H.: 2012, The relation between coronal holes and coronal mass ejections during the rise, maximum, and declining phases of Solar Cycle 23. *J. Geophys. Res.* **117**. DOI.

Möstl, C., Farrugia, C.J., Kilpua, E.K.J., Jian, L.K., Liu, Y., Eastwood, J., Harrison, R.A., Webb, D.F., Temmer, M., Odstrcil, D., Davies, J.A., Rollett, T., Luhmann, J.G., Nitta, N., Mulligan, T., Jensen, E.A., Forsyth, R., Lavraud, B., De Koning, C.A., Veronig, A.M., Galvin, A.B., Zhang, T.L., Anderson, B.J.: 2010, Multi-point shock and flux rope analysis of multiple interplanetary coronal mass ejections around 2010 August 1 in the inner heliosphere. *Astrophys. J.* **758**(1), 10. DOI.

Nieves-Chinchilla, T., Vourlidas, A., Stenborg, G., Savani, N.P., Koval, A., Szabo, A., Jian, L.K.: 2013, Inner heliospheric evolution of a "stealth" CME derived from multi-view imaging and multipoint in-situ observations. I. Propagation to 1 AU. *Astrophys. J.* **779**, 55. DOI.

Nitta, N.V., Aschwanden, M.J., Freeland, S.L., Lemen, J.R., Wulser, J.-P., Zarro, D.M.: 2014, The association of solar flares with coronal mass ejections during the extended solar minimum. *Solar Phys.* **289**, 1257. DOI.

Olmedo, O., Zhang, J., Wechsler, H., Poland, A., Borne, K.: 2008, Automatic detection and tracking of coronal mass ejections in coronagraph time series. *Solar Phys.* **248**, 485. DOI.

Owens, M.J., Schwadron, N.A., Crooker, N.U., Hughes, W.J., Spence, H.E.: 2007, Role of coronal mass ejections in the heliospheric Hale cycle. *Geophys. Res. Lett.* **34**, L06104. DOI.

Reames, D.V.: 1999, Particle acceleration at the Sun and in the heliosphere. *Space Sci. Rev.* **90**, 413. DOI.

Richardson, I.G., Cane, H.V.: 1995, Regions of abnormally low proton temperature in the solar wind (1965 – 1991) and their association with ejecta. *J. Geophys. Res.* **100**, 23,397.

Richardson, I.G., Cane, H.V.: 2010, Near-Earth interplanetary coronal mass ejections during solar cycle 23 (1996 – 2009): catalog and summary of properties. *Solar Phys.* **264**, 189. DOI.

Riley, P., Schatzman, C., Cane, H.V., Richardson, I.G., Gopalswamy, N.: 2006, On the rates of coronal mass ejections: remote solar and in situ observations. *Astrophys. J.* **647**, 648.

Robbrecht, E., Berghmans, D.: 2004, Automated recognition of coronal mass ejections (CMEs) in near-real-time data. *Astron. Astrophys.* **425**, 1097. DOI.

Robbrecht, E., Patsourakos, S., Vourlidas, A.: 2009, No trace left behind: stereo observation of a coronal mass ejection without low coronal signatures. *Astrophys. J.* **701**, 283. DOI.

Rodriguez, L., Mierla, M., Zhukov, A.N., West, M., Kilpua, K.E.J.: 2011, Linking remote-sensing and in situ observations of coronal mass ejections using STEREO. *Solar Phys.* **70**, 561. DOI.

Schwenn, R., Dal Lago, A., Huttunen, K.E.J., Gonzalez, W.D.: 2005, The association of coronal mass ejections with the effects of their counterparts near the Earth. *Ann. Geophys.* **23**, 1033.

Sheeley, N.R. Jr., Lee, D.D.-H., Casto, K.P., Wang, Y.-M., Rich, N.B.: 2009, The structure of streamer blobs. *Astrophys. J.* **694**, 1471. DOI.

St. Cyr, O.C., Howard, R.A., Sheeley, N.R., Plunkett, S.P., Michels, D.J., Paswaters, S.E., Koomen, M.J., Simnett, G.M., Thompson, B.J., Gurman, J.B., Schwenn, R., Webb, D.F., Hildner, E., Lamy, P.L.: 2000, Properties of coronal mass ejections: SOHO LASCO observations from January 1996 to June 1998. *J. Geophys. Res.* **105**(A8), 18169. DOI.

Thernisien, A.F.R., Howard, R.A., Vourlidas, A.: 2006, Modeling of flux rope coronal mass ejections. *Astrophys. J.* **652**, 763.

Thernisien, A.F.R., Vourlidas, A., Howard, R.A.: 2009, Forward modeling of coronal mass ejections using STEREO/SECCHI data. *Solar Phys.* **256**, 111. DOI.

Tsurutani, B.T., Echer, E., Gonzalez, W.D.: 2011, The solar and interplanetary causes of the recent minimum in geomagnetic activity (MGA23): a combination of midlatitude small coronal holes, low IMF BZ variances, low solar wind speeds and low solar magnetic fields. *Ann. Geophys.* **29**, 839. DOI.

Vourlidas, A., Howard, R.A.: 2006, The proper treatment of coronal mass ejection brightness: a new methodology and implications for observations. *Astrophys. J.* **642**(2), 1216. DOI.

Vourlidas, A., Howard, R.A., Esfandiari, E., Patsourakos, S., Yashiro, S., Michalek, G.: 2011, Erratum: "Comprehensive analysis of coronal mass ejection mass and energy properties over a full solar cycle". *Astrophys. J.* **730**, 1.

Vourlidas, A., Lynch, B.J., Howard, R.A., Li, Y.: 2013, How many CMEs have flux ropes? Deciphering the signatures of shocks, flux ropes, and prominences in coronagraph observations of CMEs. *Solar Phys.* **284**, 179. DOI.

Wood, B.E., Howard, R.A.: 2009, An empirical reconstruction of the 2008 April 26 coronal mass ejection. *Astrophys. J.* **702**(2), 901. DOI.

Wood, B.E., Howard, R.A., Socker, D.G.: 2010, Reconstructing the morphology of an evolving coronal mass ejection. *Astrophys. J.* **715**, 1524. DOI.

Wülser, J.-P., Lemen, J.R., Tarbell, T.D., Wolfson, C.J., Cannon, J.C., Carpenter, B.A., Duncan, D.W., Gradwohl, G.S., Meyer, S.B., Moore, A.S., Navarro, R.L., Pearson, J.D., Rossi, G.R., Springer, L.A., Howard, R.A., Moses, J.D., Newmark, J.S., Delaboudini'er, J.-P., Artzner, G., Auch'ere, F., Bougnet, M., Bouyries, P., Bridou, F., Clotaire, J.-Y., Colas, G., Delmotte, F., Jerome, A., Lamare, M., Mercier, R., Mullot, M., Ravet, M.-F., Song, X., Bothmer, V., Deutsch, W.: 2004, EUVI: The STEREO-SECCHI extreme ultraviolet imager. In: Fineschi, S., Gummin, M.A. (eds.) *SPIE* **5171**. DOI.

Yashiro, S., Michalek, G., Gopalswamy, N.: 2008, A comparison of coronal mass ejections identified by manual and automatic methods. *Ann. Geophys.* **26**, 3103.

Yashiro, S., Gopalswamy, N., Michalek, G., Howard, R.A.: 2003, Properties of narrow coronal mass ejections observed with LASCO. *Adv. Space Res.* **32**(12), 2631.

Yashiro, S., Gopalswamy, N., Michalek, G., St. Cyr, O.C., Plunkett, S.P., Rich, N.B., Howard, R.A.: 2004, A catalog of white light coronal mass ejections observed by the SOHO spacecraft. *J. Geophys. Res.* DOI.

Zhang, J., Richardson, I.G., Webb, D.F., Gopalswamy, N., Huttunen, E., Kasper, J.C., Nitta, N.V., Poomvises, W., Thompson, B.J., Wu, C.-C., Yashiro, S., Zhukov, A.N.: 2005, Solar and interplanetary sources of major geomagnetic storms (Dst ≤ -100 nT) during 1996 – 2005. *J. Geophys. Res.* **112**. DOI.

Zhukov, A.N.: 2007, Using CME observations for geomagnetic storm forecasting. In: Lilensten, J. (ed.) *Space Weather: Research Towards Applications in Europe 2nd European Space Weather Week*, *Astrophys. Space Sci. Lib.* **344**. DOI.

Zurbuchen, T.H., Richardson, I.G.: 2006, In-situ solar wind and magnetic field signatures of interplanetary coronal mass ejections. *Space Sci. Rev.* **123**, 1572.